

LEVIS: Large Exact Verifiable Input Spaces for Neural Networks

Mohamad Fares El Hajj Chehade^{1,2}, Brian Wesley Bell², Russell Bent², Hao Zhu¹, Wenting Li²

¹ Chandra Department of Electrical and Computer Engineering, The University of Texas at Austin, Austin, TX, USA

² Los Alamos National Laboratory, Los Alamos, NM, USA

chehade@utexas.edu, bwbell@lanl.gov, rbent@lanl.gov, haozhu@utexas.edu, wenting@lanl.gov

Abstract

The robustness of neural networks is paramount in safety-critical applications. While most current robustness verification methods assess the worst-case output under the assumption that the input space is known, identifying a verifiable input space \mathcal{C} , where no adversarial examples exist, is crucial for effective model selection, robustness evaluation, and the development of reliable control strategies. To address this challenge, we introduce a novel framework, LEVIS, comprising LEVIS- α and LEVIS- β . LEVIS- α locates the largest possible verifiable ball within the central region of \mathcal{C} that intersects at least two boundaries. In contrast, LEVIS- β integrates multiple verifiable balls to encapsulate the entirety of the verifiable space comprehensively. Our contributions are threefold: (1) We propose LEVIS equipped with three pioneering techniques that identify the maximum verifiable ball and the nearest adversarial point along collinear or orthogonal directions. (2) We offer a theoretical analysis elucidating the properties of the verifiable balls acquired through LEVIS- α and LEVIS- β . (3) We validate our methodology across diverse applications, including electrical power flow regression and image classification, showcasing performance enhancements and visualizations of the searching characteristics.

Introduction

In the last several years, Artificial Intelligence (AI) has seen extraordinary growth in the number of areas where it has demonstrated substantial impact. Despite these successes, in many areas such as safety-critical applications, the adoption of AI has seen slow or limited growth. A barrier to such adoption is robustness, as incorrect output and predictions in these settings can have severe consequences. For instance, in electrical grids, where AI models are increasingly suggested for complex controls and operations, bad output can lead to disastrous failures such as cascading blackouts. Consequently, AI has largely been restricted to academic exercises and undeployed prototypes.

One promising approach to overcome the adoption challenges associated with robustness is the analysis of the inputs to AI models. A main example is identifying *verifiable input spaces* where outputs are guaranteed to meet specific criteria, such as physical constraints or accuracy requirements (Kotha et al. 2024; Sundar et al. 2023). In this paper,

Copyright © 2025, Association for the Advancement of Artificial Intelligence (www.aaai.org). All rights reserved.

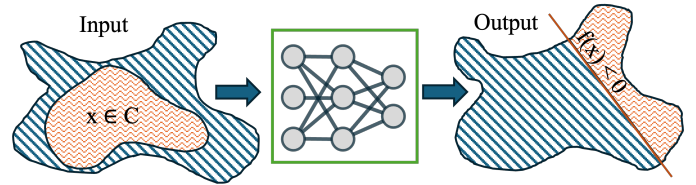


Figure 1: The verifiable input space (Orange) is \mathcal{C} consisting of the inputs $x \in \mathcal{C}$ that produce outputs satisfying the condition $f(x) > 0$ determined by the red line. Note: the left orange space may only be a subset of the pre-image of the right orange space.

we contribute to this line of research by identifying verifiable input spaces for a specific, but widely used, class of AI models—neural networks (NN).

Currently, verification of neural network (VNN) primarily focuses on checking whether the *outputs* of NNs are correct in worst-case scenarios within well-defined input domains (Tjeng, Xiao, and Tedrake 2017; Goyal et al. 2018). Techniques vary from accurately determining worst-case outputs by transforming nonlinear activation functions into integer inequality constraints, to approximating lower output bounds using linear (Wang et al. 2021) or quadratic (Kuvshinov and Günemann 2022) approximations. More sophisticated methods integrate advanced optimization approaches like bound tightening and improve computational efficiency through parallel processing (Zhang et al. 2022). Such methods place the responsibility of identifying input domains on the user and neglect thorough assessments of the inputs, probably resulting in either an underestimation or overestimation of the robust input region.

Unfortunately, such assessments of *input spaces* have received limited attention, with only a few studies exploring how far inputs can be perturbed without leading to incorrect outputs (Peck et al. 2017), while recent efforts focused on approximating the convex hull of verifiable spaces with guarantees (Kotha et al. 2024). As shown in Figure 1, one of the biggest challenges is that the verifiable input spaces, e.g. \mathcal{C} , can take any shape, and outputs satisfy a specification, e.g., $f(x) > 0$, as denoted by the red line. This challenge is even harder when trying to find the *largest* input space, as such a space is unlikely to be convex.

This paper introduces an innovative searching framework LEVIS for finding Large Verifiable Input Spaces for neural networks, which comprises two components: LEVIS- α and LEVIS- β . While LEVIS- α finds the single large verifiable ball that intersects the true space \mathcal{C} at two boundaries, LEVIS- β aims to build a collection of verifiable balls that extensively cover the verifiable input space. Crucial to both these algorithms is that every point inside the obtained regions by LEVIS is guaranteed to be verifiable. This is ensured by formulating new optimization problems to precisely calculate a maximum verifiable ball and identify adversarial examples along certain directions. In short, our main contributions include:

1. Developing an optimization model to accurately locate a maximum verifiable ball at a known center, using mixed integer programming (MIP), to guarantee the global optimal solution. Our method reveals significantly larger verifiable areas compared to the state-of-the-art methods such as those estimated with the Lipschitz constant (Ducotterd et al. 2022; Leino, Wang, and Fredrikson 2021; Fazlyab, Morari, and Pappas 2021).
2. Incorporating directional constraints, collinear and orthogonal, to identify the geometric arrangement of adversarial data points.
3. Proposing two search strategies, LEVIS- α and LEVIS- β , designed to identify large exact verifiable balls within a bounded space. LEVIS- α aims to locate the largest verifiable ball, centered near the central area of the verifiable space, effectively capturing the most substantial single verifiable region. In contrast, LEVIS- β focuses on aggregating a collection of verifiable balls to cover the entire verifiable space.
4. Demonstrating the effectiveness of our approaches on two NN applications, electric power flow regression, and image classification tasks, and visualizing the characteristics of the searched verifiable balls.

Background and Related Work

Preliminary Notation We use \mathcal{C} and \mathcal{V} to denote the verifiable spaces and the union of verifiable balls, respectively. $\mathcal{B}(c)$ represents a ball centered at c . The vector e_k is a basis vector where the k -th position is 1 and all others are 0. The $\|x\|_p$ norm is defined as $\sum_{i=1}^d (|x_i|^p)^{1/p}$, $p = 1, 2$, and $\|x\|_\infty = \max_i |x_i|$. We define an L -layer rectified linear (ReLU) neural network, where the layer i (for $i = 1, \dots, L$) uses weights $W^i \in \mathbb{R}^{d_i \times d_{i-1}}$ and biases $\beta^i \in \mathbb{R}^{d_i}$. The pre-activation and post-activation outputs for layer i are given by $z^i = W^i z^{i-1} + \beta^i$ and $\hat{z}^i = \text{ReLU}(z^i) = \max(z^i, 0)$, respectively. The input \hat{z}^0 equals the input data $x \in \mathbb{R}^{d_0}$, and the output of the network is $f(x) = z^L \in \mathbb{R}^{d_L}$.

Bounds on the Output Domain: Verification of Neural Networks Bounding the outputs of neural networks (NNs) is an effective way to verify the robustness of neural networks and enhance their reliability. In verified neural networks, given an input region \mathcal{C} , the output must meet predefined specifications \mathcal{P} to guarantee robustness. Neural network verification involves solving an optimization problem

where $f^* = \min_{x \in \mathcal{C}} f(x)$, subject to the $\hat{z}^0 = x$, $z^i = W^i \hat{z}^{i-1} + \beta^i$, $\hat{z}^i = \max(z^i, 0)$ for $i = 1, \dots, L$, and the input domain $\mathcal{C} = \|x - x_0\|_\infty \leq \varepsilon$ is known. The network is verified if $\mathcal{P} = f^* > 0$. Verification of neural networks is NP-complete (Katz et al. 2017), primarily due to nonlinear activation functions. Solution approaches can be categorized into three types: exact or complete verifiers (Tjeng, Xiao, and Tedrake 2017), approximate or incomplete verifiers (Gowal et al. 2018; Wang et al. 2021), and probabilistic verifiers (Grunbacher et al. 2021). Unlike these methods which focus on confirming output correctness for a known input domain, our work prioritizes input domain analysis to identify the largest possible region that yields verifiable outputs, ensuring all points within this region meet the satisfaction criteria.

Bounds on the Input Domain: Robustness to Adversarial Perturbations Inputs that lead to erroneous NN outputs when perturbed are termed *adversarial examples*. The set without any adversarial examples constitutes a *verifiable input region*, understanding which is imperative for robust model selection and training (Kuvshinov and Gunnemann 2022; Kotha et al. 2024). Early efforts to gauge this region involved approximating the closest distance to adversarial perturbations via quadratic programming (Kuvshinov and Gunnemann 2022), while other studies derived theoretical lower bounds for the norm of adversarial perturbations (Peck et al. 2017). These approaches primarily focused on the magnitude of perturbations rather than the distribution ranges of the perturbations, aiding only in local robustness assessments and not in understanding the global characteristics of the verifiable region. Recently, the analysis of the verifiable input region has attracted more attention, particularly for physical problems that must demonstrably satisfy specific properties. Novel CROWN-based optimization solvers have been developed to determine the convex hull of the verifiable input region (Kotha et al. 2024). However, such a method provides an *overapproximation* of the input region. Therefore, some points inside the obtained convex hull may not be verifiable.

Problem Formulation

A *verifiable space* comprises input data points for neural networks that only yield verifiable outputs. Our objective is to precisely identify large verifiable spaces, which are crucial for model selection, robustness evaluation, and safe control operations (Kotha et al. 2024). The challenge lies in maximizing the verifiable input space \mathcal{C} , where arbitrary data points in the set \mathcal{C} generate verifiable outputs with guarantees, formalized as $\max_{\mathcal{C}} \min_{x \in \mathcal{C}} f(x) > 0$. This task fundamentally constitutes an intractable min-max optimization problem, especially when the verifiable space is non-convex.

To manage this complexity, we propose approximating these verifiable spaces using one or more verifiable balls. A ball is defined by distinct centers and radii, ensuring that all data points within this ball, when input to the neural network, provide verifiable outputs. Crucial to our approach is the identification of appropriate centers and radii that guarantee (1) the verifiability of interior data points and (2) the substantial coverage of the verifiable input space.

Approach

Our method begins by precisely identifying a maximal verifiable ball centered at a given point x_0 , and then iteratively shifts the center to either identify a large boundary-touching verifiable ball or assemble a large union of such verifiable balls.

Find the Maximum Verifiable Input Ball around c

We find the maximum verifiable ball around center c by locating the **nearest adversarial data point** x^* . This point lies on the boundary of the verifiable input space and yields a violating output $f(x^*) \leq 0$. The optimization problem for finding x^* is structured as follows:

$$\min_x \|x - c\|_p \quad (1a)$$

$$\text{subject to } \hat{z}^0 = x \quad (1b)$$

$$\hat{z}^{(i)} = \sigma(z^{(i)}) \quad (1c)$$

$$z^i = W^i \hat{z}^{(i-1)} + \beta^i \quad (1d)$$

$$f(x) = z^L \quad (1e)$$

$$f(x) < 0, i \in \{1, \dots, L\} \quad (1f)$$

Equation (1e) defines the output property, while (1f) ensures the solution violates the specified output condition. The objective function in (1a) seeks the nearest adversarial point x in the l_p -norm distance from c . This optimization is treated as a mixed-integer program (MIP), solvable via standard optimization tools to achieve the global optimum. The verifiable ball, denoted as $\mathcal{B}(c)$, is characterized by the center c . All points inside $\mathcal{B}(c)$ are guaranteed to produce verifiable outputs, confirming x^* as the nearest adversarial example.

We introduce our search methodologies, termed Large Exact Verifiable Input Spaces (LEVIS), which employ two strategies based on the exact maximum verifiable ball as defined in (1). The first strategy, LEVIS- α identifies a large verifiable ball intersecting at least two boundaries of the verifiable input spaces. The approach involves adjusting the center of each verifiable ball towards the central area of the verifiable input space by averaging adversarial points on the boundary along different directions. The second strategy, LEVIS- β , focuses on approximating the unknown verifiable input spaces through a union of verifiable balls. This method ensures the verifiability of the center while strategically relocating it beyond the existing verifiable balls, moving towards more inclusive areas of the input space.

LEVIS: Large Exact Verifiable Input Spaces for Neural Networks

(1) LEVIS- α : Search for the Large Boundary-Touching Verifiable Ball

The core technique of this searching strategy is to average the d pairs of boundary adversarial points b_{2j+1} and b_{2j+2} , $j = 0, \dots, d-1$ obtained by solving the minimization in (1) with the directional constraints. Specifically, we add two kinds of constraints to the original optimization problem in (1) that guide the search direction. Given the

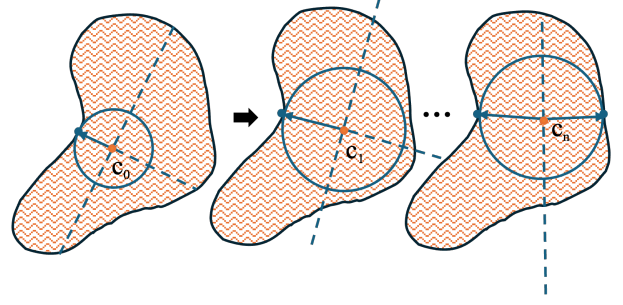


Figure 2: Illustration of the sequence of balls centered at the red points c_0, \dots, c_n obtained by LEVIS- α , where the arrows point to the nearest adversarial points that define the radius of those balls. The searching converges at the final ball $\mathcal{B}(c_n)$ touching at least two boundaries of the bounded verifiable input spaces.

center of the previous ball c and the closest adversarial point b_{2j+1} , we can find another adversarial point b_{2j+2} along the direction of $\overrightarrow{b_{2j+1}, c}$. Precisely,

$$\min_{b_{2j+2}, k < 0} \|b_{2j+2} - c\|_p \quad (2a)$$

$$\text{subject to } (1b) - (1f), x = b_{2j+2} \quad (2b)$$

$$b_{2j+2} - c = k(b_{2j+1} - c), k < 0 \quad (2c)$$

Note the (2c) represents the **collinear constraint** that ensures the new adversarial point is assigned linearly with the previous adversarial point.

Similarly, we can find another adversarial boundary point b_{2j+1} in the j th dimension, such that $\overrightarrow{b_{2j+1}, c}$ is orthogonal to $\overrightarrow{b_{2j-1}, c}$. We replace the directional constraint in (2c) with the orthogonal constraint $(b_{2j+1} - c)^T (b_{2j-1} - c) = 0$. The new optimization problem is shown below, while the detailed algorithm, termed LEVIS- α is described in Algorithm 1 and is illustrated in Figure 2.

$$\min_{b_{2j+1}} \|b_{2j-1} - c\|_p \quad (3a)$$

$$\text{subject to } (1b) - (1f), x = b_{2j-1} \quad (3b)$$

$$(b_{2j+1} - c)^T (b_{2j-1} - c) = 0 \quad (3c)$$

Note the (3c) denotes the **orthogonal constraint** that guides the searching toward the orthogonal direction to find the next adversarial point.

The Algorithm 1 updates the center of the verifiable ball in each iteration and eventually converges to a large exact verifiable ball at the central area of the verifiable space, touching two adversarial points, as illustrated in Figure 2. In each iteration, the algorithm searches d pairs of adversarial points along the collinear and orthogonal directions respectively. The below theorem shows the final ball touches at least two boundaries of the verifiable spaces when certain conditions are met:

Theorem 1. For any bounded verifiable region $\mathcal{C} \subset \mathbb{R}^d$, the sequence of balls $\{\mathcal{B}(c_n)\}$ generated by LEVIS- α converges to a ball $\mathcal{B}(c)$ that intersects the boundary of \mathcal{C} at

Algorithm 1: LEVIS- α : Iterative Refinement for Center Estimation

- 1: **initialize:** Given the original data x_0 as the ball center $c = x_0, r = \infty, r_{\text{old}} = 0$, tolerance $\epsilon > 0$, the weights and bias of the neural networks $\Theta = \{W^i, \beta^i, i = 1, \dots, L\}$.
 - 2: **while** $\|r - r_{\text{old}}\| \geq \epsilon$ **do**
 - 3: $b_1 \leftarrow$ Solve (1).
 - 4: The radius $r = \|b_1 - c\|_p$
 - 5: $b_2 \leftarrow$ Solve (2) with $j = 0$.
 - 6: **for** $j = 1$ to $d - 1$ **do**
 - 7: $b_{1+2j} \leftarrow$ Solve (3) along the orthogonal direction
 - 8: $b_{2+2j} \leftarrow$ Solve (2) along the collinear direction
 - 9: **end for**
 - 10: $c \leftarrow \frac{1}{2d} \sum_{l=1}^{2d} b_l, r_{\text{old}} \leftarrow r$
 - 11: **end while**
 - 12: **Return** c, r
-

least at two points. Specifically, for any $\epsilon > 0$, there exists an N such that for all $n > N$, $\mathcal{B}(c)$ encompasses two points almost symmetric about the center c with less than ϵ mismatch, and these two points lie on the boundary of \mathcal{C} .

The underlying rationale is that LEVIS- α progressively averages the collinear adversarial pairs (b_{2j+1}, b_{2j+2}) (where $l = 0, \dots, d - 1$) through $c = \frac{1}{2d} \sum_{l=1}^{2d} b_l$, thereby minimizing the asymmetry between each pair of collinear adversarial points (b_{2j+1}, b_{2j+2}) to the new center in subsequent iterations. Given that \mathcal{C} is bounded, the movement of the ball ceases once at least one pair of adversarial points (b'_1, b'_2) touches the surface of the ball, while other pairs become symmetric relative to the center c with less than ϵ mismatch. Hence, the ball ultimately intersects the boundary of \mathcal{C} at at least two distinct points. The complete proof is provided in the appendix.

(2) LEVIS- β : Collect the Large Union of Verifiable Balls

This searching strategy also moves the center inside the search space. Every time a center is found, a new region is obtained by solving (1). Nonetheless, unlike LEVIS- α , each new region encountered is saved inside a set \mathcal{V} . In other words, the final region obtained is a union of all the regions encountered during the search. The innovative idea of this searching strategy is looking for a verifiable new center outside the known verifiable union by extensively moving towards all orthogonal directions. Specifically, by solving (1) and (3), we obtain a verifiable ball $\mathcal{B}(c)$ centered at c and the nearest adversarial orthogonal point b . Once a new ball $\mathcal{B}(c)$ is found, we define the new center to be the middle point that lies in the same line with c, b but outside $\mathcal{B}(c)$, as shown in the equation (4), and as illustrated in Figure 3.

$$m = \frac{z + b}{2}, z = c - \frac{c - b}{\|c - b\|_p} \cdot r \quad (4)$$

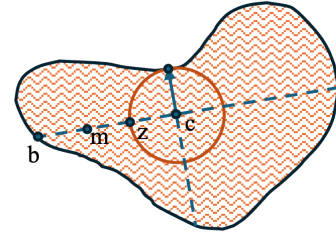


Figure 3: Illustration of the geometric position of the middle point defined by Eq. (4).

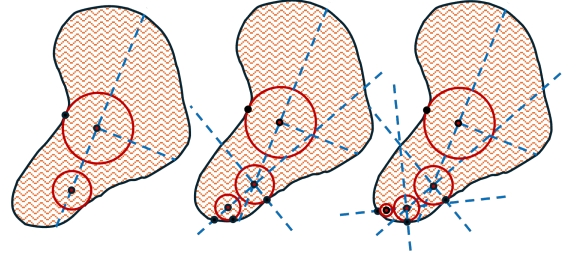


Figure 4: LEVIS- β searches for the union of verifiable balls to cover the verifiable input space until the uncovered gap is less than ϵ -balls.

Our new Algorithm 2, termed LEVIS- β maintains the verifiability of the center while searching in orthogonal directions for external balls outside the known union of verifiable balls. Step 4 ensures that the newly identified adversarial point b_{j+1} is verifiable along the direction orthogonal to $\overrightarrow{b_j, c}$. Step 5 computes a verifiable midpoint outside the prior ball centered at c with radius r . Steps 6-8 adjust the position of m towards b_{j+1} if it lies within the existing union of verifiable balls. The algorithm systematically searches through all d dimensions of the input data through the loop in Steps 3-11 to identify verifiable balls and terminates when the radius of a verifiable ball is less than ϵ . Figure 4 illustrates the growth of the union with iterations, where the blue imaginary lines denotes the searching directions and the red circles represent the verifiable balls in the union.

Remark: We assert that the new center c remains a verifiable point during the execution of Algorithm 2. Given that $\overrightarrow{b_{j+1}}$ is the nearest adversarial point along the vector $\overrightarrow{b_{j+1}, c}$, it follows that any point closer to the center c along this vector than b_{j+1} is verifiable. The middle point, as defined by steps 5-8 in Algorithm 2, is such a point and is therefore verifiable. Meanwhile, we emphasize that the center c is positioned outside the existing union of verifiable balls. This positioning ensures that the total volume of the union increases progressively throughout the search process.

Experiments

We implement our algorithms on two benchmark systems, tailored to the specific requirements of physical limits and robust accuracy. We utilize three-layer dense neural networks to model solutions for optimal power (regression) and image classification tasks, employing PyTorch (Imambi,

Algorithm 2: LEVIS- β : External Ball Searching in Orthogonal Directions

```

1: initialize: Given  $x_0$ ,  $\epsilon > 0$ , and  $\Theta = \{W^i, \beta^i, i = 1, \dots, L\}$ ; Initialize the set of verifiable balls  $\mathcal{V} = \emptyset$ ,  $c = x_0$ ; solve (1) to obtain the optimal solution  $b_0$ ; define  $B(c)$  with radius  $r = \|b_0 - c\|_p$  centered at  $c$ , and add the ball to the set  $\mathcal{V} = \mathcal{V} \cup \{(c, r)\}$ .
2: while  $r \geq \epsilon$  do
3:   for  $j = 0$  to  $d - 1$  do
4:     Find  $b_{j+1}$  by solving (3) with the orthogonal constraint  $(b_{j+1} - c)^T (b_j - c) = 0$ 
5:     Utilize  $c, b_{j+1}, r$  to compute  $m$  following (4)
6:     while  $m \in \mathcal{V}$  and  $\|m - b_{j+1}\|_p > \epsilon$  do
7:        $m = (m + b_{j+1})/2$ 
8:     end while
9:      $c = m, r = \|c - b_{j+1}\|_p$ 
10:    Update  $\mathcal{V} = \mathcal{V} \cup \{(c, r)\}$ 
11:   end for
12: end while
13: Return  $\mathcal{V}$ 

```

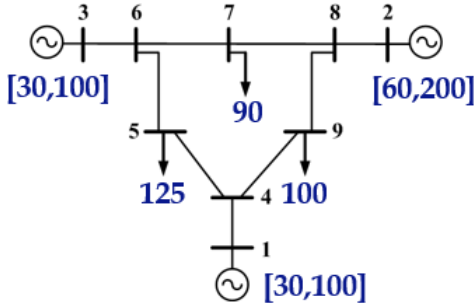


Figure 5: IEEE 9-Bus system topology (Fernandez and Go 2023). The system has 3 demand nodes (5,7,9) with nominal values (125, 90, 100) in MW, and the 3 generator nodes with (1,2,3) with limits ([30,100], [60,200], [30,100]) in MW. Therefore, the neural network has 3 inputs and 3 outputs.

Prakash, and Kanagachidambaresan 2021) for development. To validate the neural networks, we convert the trained models into the Open Neural Network Exchange (ONNX) format and employ OMLT (Ceccon et al. 2022), a library for representing neural networks in optimization problems. For the mixed-integer programming (MIP) optimization tasks in (1), (2), and (3), we leverage major MIP solvers including the open-source options CBC (Forrest and Lougee-Heimer 2005), GLPK (Makhoriin 2023), Bonmin (Bonami et al. 2023), and SCIP (SCIP Team 2024). The optimization problems are modeled in PYOMO (Hart et al. 2024). We plan to release our code and datasets publicly at <https://github.com/LEVIS>.

Dataset I and Implementation for DC-OPF

We generate direct-current (DC) power flow datasets using the IEEE 9-bus power grid benchmark, a widely recognized model for simulating energy flow in power grids

(PSCAD 2024), depicted in Figure 5. The neural network, $f_{\text{opf}}(P_D) = P_G$, predicts the electricity generated (P_G) at these three generator nodes based on the demand (P_D) from the load nodes and $P_D \in \mathbb{R}^3$. The dataset is created by solving the DC Optimal Power Flow (DC-OPF) problem (Frank, Steponavice, and Rebennack 2012) using nominal inputs $x_0 = [125, 90, 100]^T$ from standard datasets, perturbed by 10% uniform noise to produce a diverse set of 1,000 data samples. The DC-OPF specification requires that outputs stay within the physical limits of the generators, specifically $P_{G1} \in [30, 100]$, $P_{G2} \in [60, 200]$, and $P_{G3} \in [30, 100]$. We trained a three-layer ReLU neural network using the Adam optimizer (Kingma and Ba 2014) to compute DC-OPF solutions, selecting 80% of the data samples randomly for training and reserving the remaining for testing.

Dataset II and Implementation for Images

We utilize the MNIST digit dataset, which consists of 60,000 training and 10,000 testing samples, for an image recognition task (LeCun, Cortes, and Burges 2010). This dataset comprises handwritten digits across ten classes (0 to 9). The neural network $f_{\text{image}}(x) = \hat{y}$, predicts class probabilities for each input x . The primary objective in image classification is to ensure that the predicted probability for the actual class k exceeds that of any other class, operationalized as $\min_{k \neq l} (e_k - e_l)^T f_{\text{image}}(x)$. We implement a two-layer ReLU neural network using a cross-entropy loss function and optimize it using the Adam optimizer with a learning rate of 0.001. Given that the original input dimensions are 28×28 and exhibit low-rank characteristics, we employ principal component analysis (PCA) to reduce input dimensions from 728 to 50 without significantly compromising accuracy but accelerating the training efficiency about 1560 times (Murphy 2022). Details of our model reduction methodology and analysis are presented in the appendix.

Visualization of the exact verifiable ball

To rigorously analyze the properties of maximum verifiable balls centered at x_0 , we examined individual verifiable balls $\mathcal{B}(x_0)$ across norms l_p where $p = 1, 2, \infty$, by solving the minimization in (1). Figure 6 illustrates the verifiable balls using the DC-OPF datasets centered at $x_0 = [125, 90, 100]$. The l_1 -norm ball exhibits the smallest radius, whereas the l_∞ -norm ball presents the largest within this dataset. Notably, although adversarial points, represented as red nodes in Figure 6, occur at the vertices of these balls, not all vertices necessarily represent adversarial points. Our solution in (1) ensures that any point closer to x_0 than x^* , or inside the ball, is verifiable, yet points equidistant from x_0 to x^* are potentially adversarial. For instance, in the l_∞ -norm ball, adversarial points may exist anywhere on the surface, rather than solely at discrete vertices or edges; in contrast, for the l_2 -norm ball, while adversarial points occur only at vertices, these vertices are infinitely numerous. This insight underscores the challenges in search methods that aim to expand the union of verifiable balls by enumerating vertices or edges. Our approach instead explores favorable directions to identify new balls.

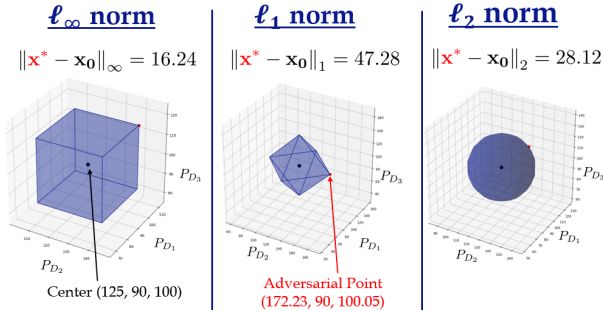


Figure 6: Single maximum verifiable balls obtained by solving (1) with different norms using DC-OPF datasets. Note that the center is $x_0 = [125, 90, 100]$ and the nearest adversarial points x^* are denoted as red nodes. $\|x^* - x_0\|_p$ represents the radius or the smallest distance between the adversarial point and the center. Since the input space is 3D, the regions obtained by ℓ_∞ , ℓ_1 and ℓ_2 norms (left to right) are respectively a cube, an octahedron, and a sphere.

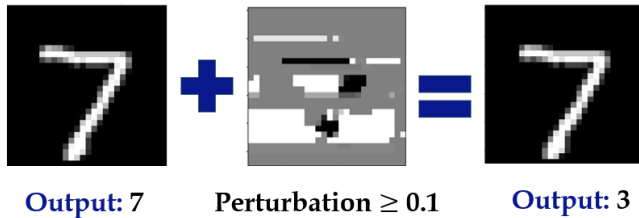


Figure 7: The minimum perturbation needed to the clean image of “7” (on the left) has a value of 0.1 and is shown in the center image. This results in an image (on the right) that is visually very close, but the classifier mistakes it for the digit “3”.

For image recognition, we find the closest adversarial point to the clean image of the digit “7”, in Figure 7. The distance to the adversarial point was 0.1.

Comparison of the radius size with the baseline

We compare the size of the ball obtained in the earlier section with the state of the art. The baseline method computes the distance $\|x - c\|_p$ in (1) using the Lipschitz constant (Fazlyab, Morari, and Pappas 2021). As neural networks prove to be Lipschitz L continuous, with $L = \prod_{i=1}^L \|W_i\|_p$, we can calculate the lower bound of the closest distance from an adversarial point to the center c by $\|x^* - c\|_p \geq \delta/L$, where $\delta = \min_{i \neq k} 1/\sqrt{2} |(e_k - e_i)^T f(x^*)|$. Table 1 shows that our method identifies verifiable balls with radii up to seven times larger than those determined by the baseline method, emphasizing the advantages of solving the exact problem in (1) rather than finding a lower bound.

Performance of LEVIS- α for DC-OPF

We implement LEVIS- α for DC-OPF and track the variations in the radius of verifiable balls, as shown in Figure 8.

Table 1: The radii obtained by solving our exact problem in (1) vs the lower bound approximation. The exact problem produces regions with much larger radii.

Methods	$p = \infty$	$p = 1$	$p = 2$
Baseline r	6.386	6.79	18.22
Our r	16.24	47.28	28.12

To underscore the substantial size of the final verifiable ball obtained by LEVIS- α , we compare it with two alternative methods: the Exact Fixed Center (EFC) method as defined in (1), and the Lipschitz-based Lower Bound (LLB) method, described previously. Two important things are noted: first, the radius of the region obtained by LEVIS- α is 3 to 9 times larger than the other two methods, indicating the region is *large*, and therefore iteratively refining the center, as pointed out by Algorithm 1, is justifiable. Second, the radius converges to a fixed value, implying that the obtained ball intersects the true region at two distinct edges.

Performance of LEVIS- β for DC-OPF

We assess the statistical performance of LEVIS- β for DC-OPF, noting that LEVIS- β identifies verifiable balls of varying sizes across iterations, which eventually converge to smaller verifiable balls. These smaller balls are not only distanced from the original center but also proximate to the boundaries of the verifiable spaces. Figure 10 (a) enumerates the verifiable balls by radius size, while (b) maps the distribution of radii relative to their distance from the original data point x_0 . Integrating insights from both figures, it becomes evident that the smaller-radius balls, which constitute the majority of the union, are situated far from x_0 and near the verifiable space boundaries. This pattern emphasizes the tendency for smaller verifiable balls to emerge as they approach the boundary of the verifiable space. To confirm these observations, we visualize the expansion of the union over the initial four iterations in Figure 9. The radii of the balls in the first three iterations are relatively large. However, starting from the fourth iteration, the radii decrease as the verifiable balls near the boundary of the verifiable space.

LEVIS- β for MNIST

LEVIS- β is equally effective for the MNIST problem. The distribution of the radii obtained is depicted in Figure 11. Comparing these radii with those in Figure 10, the distinctive distributions effectively highlight the differing geometrical structures of the verifiable spaces between these two datasets.

Conclusion and Future Work

Verifying neural network outputs has traditionally focused on worst-case outputs for given input domains. However, the identification of verifiable input spaces free from adversarial examples offers substantial benefits for model selection, robustness evaluation, and the development of reliable control strategies. Our work pioneers the precise mapping of extensive and exact verifiable input spaces by identifying

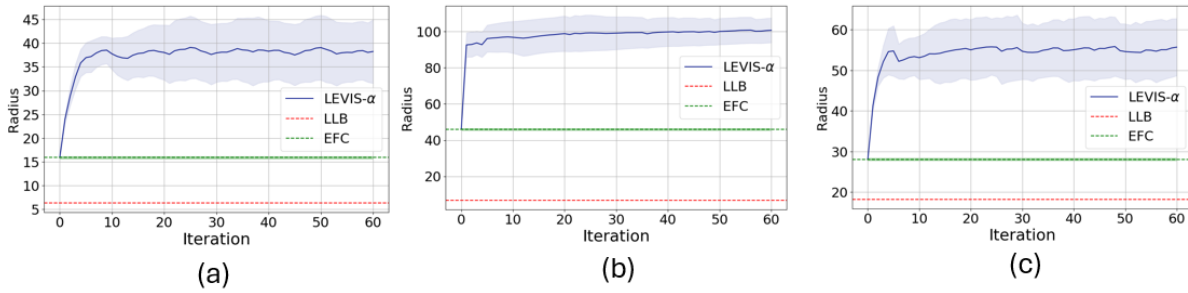


Figure 8: The radius with iterations in terms of (a) ℓ_∞ , (b) ℓ_1 and (c) ℓ_2 norms, where each strong blue line denotes the mean radius of five random implementations of LEVIS- α while the shades are the standard deviations.

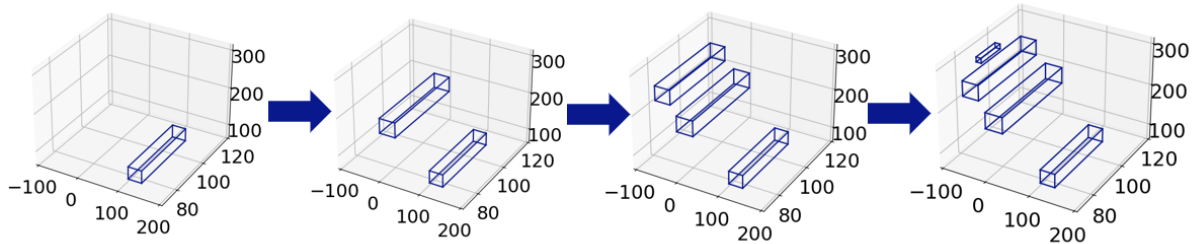


Figure 9: The verifiable regions produced in the first four invocations of LEVIS- β are square-shaped, due to the utilization of the ℓ_∞ norm. The algorithm excels in two primary aspects: (1) it generates verifiable regions that are widely distributed, effectively optimizing spatial coverage, and (2) it ensures the verifiability of the center for each new region.

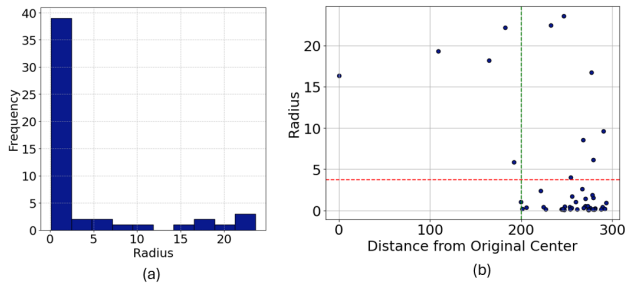


Figure 10: The distribution of the radii for LEVIS- β . (a) shows the histogram of the radii, while (b) plots the radii size as a function of the distance to the original center that the algorithm started with. Although (a) shows that most of the radii are very small in size, (b) clarifies that most of these small radii are far from the original center and probably very close to the boundary of the true verifiable region.

verifiable balls. We introduce three innovative techniques that ascertain the largest verifiable ball and locate the nearest adversarial point, whether along collinear or orthogonal directions. Utilizing these methods, we devise the search strategies LEVIS- α and LEVIS- β , which respectively identify a significant central verifiable ball and a comprehensive union of verifiable balls, ensuring these regions are free from adversarial examples.

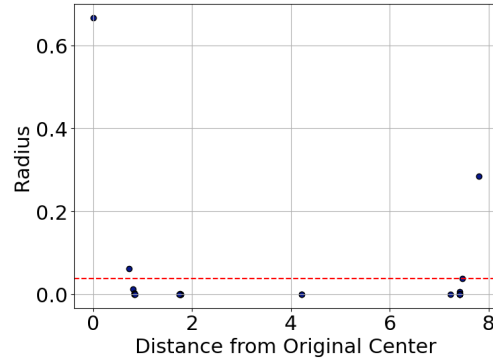


Figure 11: The distribution of the radii of the regions obtained by LEVIS- β for the MNIST problem.

We validate our approaches in regression and classification scenarios with superior performance over existing methods. We visualize and analyze single verifiable balls across various l_p norms ($p = 1, 2, \infty$) and the progressive expansion of the union of verifiable balls. These investigations not only demonstrate the geometric structure and spatial distribution of the verifiable balls but also highlight advantageous search dynamics. Motivated by these successes, we aim to refine search methodologies for large neural networks, focusing on reducing optimization counts and enhancing the speed of verifying individual balls.

References

- Bonami, P.; et al. 2023. Bonmin: Basic Open-source Non-linear Mixed Integer programming.
- Ceccon, F.; Jalving, J.; Haddad, J.; Thebelt, A.; Tsay, C.; Laird, C. D.; and Misener, R. 2022. OMLT: Optimization & Machine Learning Toolkit. *Journal of Machine Learning Research*, 23(349): 1–8.
- Ducotterd, S.; Goujon, A.; Bohra, P.; Perdios, D.; Neumayer, S.; and Unser, M. 2022. Improving Lipschitz-Constrained Neural Networks by Learning Activation Functions. *CoRR*, abs/2210.16222.
- Fazlyab, M.; Morari, M.; and Pappas, G. J. 2021. An introduction to neural network analysis via semidefinite programming. In *2021 60th IEEE Conference on Decision and Control (CDC)*, 6341–6350. IEEE.
- Fernandez, M. I.; and Go, Y. I. 2023. Power management scheme development for large-scale solar grid integration. *Journal of Electrical Systems and Information Technology*, 10(1): 15.
- Forrest, J.; and Lougee-Heimer, R. 2005. CBC user guide. In *Emerging theory, methods, and applications*, 257–277. INFORMS.
- Frank, S.; Steponavice, I.; and Rebennack, S. 2012. Optimal power flow: A bibliographic survey I: Formulations and deterministic methods. *Energy systems*, 3: 221–258.
- Gowal, S.; Dvijotham, K.; Stanforth, R.; Bunel, R.; Qin, C.; Uesato, J.; Arandjelovic, R.; Mann, T. A.; and Kohli, P. 2018. On the Effectiveness of Interval Bound Propagation for Training Verifiably Robust Models. *CoRR*, abs/1810.12715.
- Grunbacher, S.; Hasani, R.; Lechner, M.; Cyranka, J.; Smolka, S. A.; and Grosu, R. 2021. On the verification of neural odes with stochastic guarantees. In *Proceedings of the AAAI Conference on Artificial Intelligence*, volume 35, 11525–11535.
- Hart, W. E.; et al. 2024. Pyomo: Python Optimization Modeling Objects. Available at <https://www.pyomo.org>.
- Imambi, S.; Prakash, K. B.; and Kanagachidambaresan, G. 2021. PyTorch. *Programming with TensorFlow: solution for edge computing applications*, 87–104.
- Katz, G.; Barrett, C.; Dill, D.; Julian, K.; and Kochenderfer, M. 2017. Reluplex: An Efficient SMT Solver for Verifying Deep Neural Networks. *arXiv:1702.01135*.
- Kingma, D. P.; and Ba, J. L. 2014. Adam: A method for stochastic optimization. In *Proc. 3rd Int. Conf. Learn. Representations*, 1–15.
- Kotha, S.; Brix, C.; Kolter, J. Z.; Dvijotham, K.; and Zhang, H. 2024. Provably bounding neural network preimages. *Advances in Neural Information Processing Systems*, 36.
- Kuvshinov, A.; and Günnemann, S. 2022. Robustness verification of ReLU networks via quadratic programming. *Machine Learning*, 111(7): 2407–2433.
- LeCun, Y.; Cortes, C.; and Burges, C. 2010. MNIST handwritten digit database. *ATT Labs [Online]*. Available: <http://yann.lecun.com/exdb/mnist>, 2.
- Leino, K.; Wang, Z.; and Fredrikson, M. 2021. Globally-Robust Neural Networks. In Meila, M.; and Zhang, T., eds., *Proceedings of the 38th International Conference on Machine Learning, ICML 2021, 18-24 July 2021, Virtual Event*, volume 139 of *Proceedings of Machine Learning Research*, 6212–6222. PMLR.
- Makhorin, A. 2023. GLPK (GNU Linear Programming Kit).
- Murphy, K. P. 2022. *Probabilistic machine learning: an introduction*. MIT press.
- Peck, J.; Roels, J.; Goossens, B.; and Saeys, Y. 2017. Lower bounds on the robustness to adversarial perturbations. *Advances in Neural Information Processing Systems*, 30.
- PSCAD. 2024. IEEE 09 Bus System.
- SCIP Team. 2024. SCIP Optimization Suite.
- Sundar, K.; Nagarajan, H.; Misra, S.; Lu, M.; Coffrin, C.; and Bent, R. 2023. Optimization-based bound tightening using a strengthened QC-relaxation of the optimal power flow problem. In *2023 62nd IEEE conference on decision and control (CDC)*, 4598–4605. IEEE.
- Tjeng, V.; Xiao, K.; and Tedrake, R. 2017. Evaluating robustness of neural networks with mixed integer programming. *arXiv preprint arXiv:1711.07356*.
- Wang, S.; Zhang, H.; Xu, K.; Lin, X.; Jana, S.; Hsieh, C.; and Kolter, J. Z. 2021. Beta-CROWN: Efficient Bound Propagation with Per-neuron Split Constraints for Neural Network Robustness Verification. In Ranzato, M.; Beygelzimer, A.; Dauphin, Y. N.; Liang, P.; and Vaughan, J. W., eds., *Advances in Neural Information Processing Systems 34: Annual Conference on Neural Information Processing Systems 2021, NeurIPS 2021, December 6-14, 2021, virtual*, 29909–29921.
- Zhang, H.; Wang, S.; Xu, K.; Li, L.; Li, B.; Jana, S.; Hsieh, C.-J.; and Kolter, J. Z. 2022. General cutting planes for bound-propagation-based neural network verification. *Advances in neural information processing systems*, 35: 1656–1670.

Appendix

Theorem 1

Theorem 1. For any convex bounded verifiable region $C \subset \mathbb{R}^d$, the sequence of balls $\{B(c_n)\}$ generated by LEVIS- α converges to a ball $B(c)$ that intersects the boundary of C at least at two points. Specifically, for any $\varepsilon > 0$, there exists a number of algorithm iterations N such that for all $n > N$, $B(c)$ encompasses two points almost symmetric about the center c with less than ε mismatch, and these two points lie on the boundary of C .

Proof. Consider the convex, bounded, and closed region $R \subset \mathbb{R}^k$. At each step n of Algorithm 1, a ball B_{c_n, r_n} is generated, where c_n is the center and r_n is the radius, with the property that $B_{c_n, r_n} \subseteq R$. By convexity and boundedness, the boundary ∂R is non-empty, compact, and ensures that the sequence $\{B_{c_n, r_n}\}$ must converge to a configuration where the ball touches the boundary of R at multiple points.

Next, we introduce a constant λ , which we define as the greatest rate of change in the width of the region R along any line passing through its center. Specifically, λ characterizes the maximum rate at which the distance between two points on the boundary of R , on opposite sides of a line passing through the center, changes as we move the line across R . This constant λ is finite due to the convexity and boundedness of R .

Now, consider the rays emanating from the center c_n in the directions aligned with the axes of the ℓ_1 norm. The algorithm iteratively adjusts the center c_n to reduce the asymmetry of the distances from c_n to the boundary ∂R along these rays. Let Δ_n denote the measure of asymmetry at the n -th step, defined as the maximum difference between the distances from c_n to ∂R along opposite rays.

By the convexity of R , moving the center c_n results in a decrease in Δ_n at a rate proportional to the distance r_n from c_n to the boundary ∂R . Specifically, due to the convexity and the definition of λ , the reduction in Δ_n between steps n and $n + 1$ can be bounded below by $\lambda \cdot r_n$. Hence, the sequence $\{\Delta_n\}$ converges to zero as n increases.

To formalize this, given any $\varepsilon > 0$, choose N such that for all $n > N$, the asymmetry Δ_n is less than ε . The constant λ ensures that for $n > N$, the ball B_{c_n, r_n} touches the boundary ∂R at least at two distinct points, as the rays from the center are symmetrized to within ε/λ . Thus, B_{c_n, r_n} intersects ∂R at two points, say x_n and y_n , satisfying $\|x_n - y_n\|_1 \geq \frac{r_n}{2}$.

Moreover, since the asymmetry Δ_n is controlled by λ , the point b_n within B_{c_n, r_n} can be chosen such that $\|x_n - b_n\|_1 > \frac{r_n}{2}$ and $\min_{r \in R} \|b_n - r\| < \varepsilon$.

Therefore, the sequence $\{B_{c_n, r_n}\}$ converges to a ball that touches the boundary of R at at least two distinct points, which completes the proof. \square

Note: In general, for non-convex regions, this does not necessarily hold. In particular, separate convex sub-regions separated by a bottleneck can form an oscillator in this algorithm without convergence. In practice, we conjecture that this is a rare scenario and that our algorithm seems to reliably get “caught” in small convex sub-regions.

Statistical Performance of LEVIS- β

Table 2: Statistical Summary of the Radii

Statistic	Value
Number of Radii	52
Minimum Radius	0.10
Maximum Radius	23.58
Median	0.42
Mean	3.75
Lower Quartile	0.16
Upper Quartile	2.46
Variance	45.25
Standard Deviation	6.73

We provide more statistics on LEVIS- β for DC-OPF. The main results are found in Table 2.

Dimension Reduction for Speed-up Searching

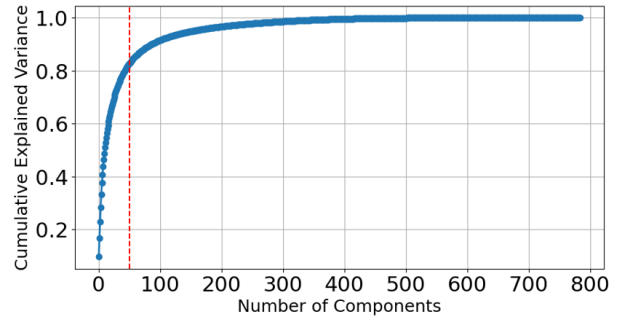


Figure 12: The variance recovered as a function of the number of principal components. The first 50 principal components recover about 85% of the variance.

Table 3: Using PCA and reducing the network size increased computation speed by a factor of 1560 while maintaining equivalent training accuracy.

Method	Accuracy	Time	Speedup
Full Dense	97%	3,120 s	-
PCA + Dense	94%	2 s	1560×

In order to reduce the dimensionality for the image recognition example, we perform Principal Component Analysis (PCA). The variance plot is shown in Figure 12. Based on the study, we see that the first 50 components can capture about 85% of the variance and are thus chosen. After reducing the dimension with PCA method, the training time is accelerated by 1560 times with simply 3% accuracy decrease as described in Table 3.